Research Inventy: International Journal of Engineering And Science
Vol.6, Issue 4 (April 2016), PP -06-18
Issn (e): 2278-4721, Issn (p):2319-6483, www.researchinventy.com

Molecular structure, vibrational, UV, NMR , molecular electrostatic surface potential and HOMO-LUMO Analysis of 1,4-dichloro-2-nitrobenzene

S.Seshadri [1], Rasheed .M.P [2]

[1](*Associate Professor and Head, PG and Research Department of Physics,Urumudhanalakshmi College ,Trichy-19)*

[2] *(Research Scholar, PG and Research Department of Physics, Urumudhanalakshmi College ,Trichy-19)*

Abstract: *The FTIR and FT Raman spectra of 1-4-Dichloro-2-NitroBenzene (14DC2NB) have been recorded in the region 4000-400 cm^{-1} and 3500-50 cm^{-1} respectively. The optimized geometry ,frequency and intensity of the vibrational bands of 1-4-Dichloro-2-NitroBenzene (14DC2NB) was obtained by the Density functional theory (DFT)using the basis set 6-31g(d,p). The harmonic vibrational frequencies were calculated and scaled values have been compared with experimental FT-IR and FT-Raman spectra. The Calculated and Observed frequencies are found to be in good agreement. UV-Visible spectrum of the compound was recorded, the electronic properties and HOMO - LUMO energies were calculated by Time Dependent DFT (TD-DFT) approach. A detailed interpretation of the infrared and Raman spectra were also reported based on Potential Energy Distribution (PED). The ^{1}H and ^{13}C nuclear magnetic resonance (NMR) chemical shifts of 14DC2NB were calculated using the GIAO approach by applying B3LYP method. The calculated HOMO and LUMO energies show that charge transfer occurs within the molecule. The Chemical reactivity and Thermodynamic properties of 14DC2NB at different temperatures were also calculated.*

Keywords: *FTIR; FT-Raman; UV-Vis; NMR; Hyperpolarizability; HOMO - LUMO; 14DC2NB*

I. Introduction

Benzene and its derivatives has been the subject of investigation for many reasons. 1,4 dichloro-2-nitrobenzene (14DC2NB) is colourless organic compound with the chemical formula $C_6H_3Cl_2NO_2$. It is an isomer of dichloronitrobenzene. Aromatic compound such as benzene derivative of 1,4-dichloro-2-nitrobenzene is commonly used as a reagent for the detection and determination of nicotinic acid, nicotine amide and other pyridine compounds. It is also used in the manufacture of ozo dyes, fungicides explosives and rubber chemicals and as an algaecide in coolant water of air conditioning system of vehicles.[1]. It is also used as an intermediate for pigments, pesticides and UV absorbents in closed systems. Contact sensitizations with 1,4-dichloro-2-nitrobenzene have been used as a measure of cellular immunity.[2]

The properties of the compound 14DC2NB are given below.

Physical state : solid, Melting point: 56.6 ^{0}C , Boiling point: 261 ^{0}C, Vapor pressure :0.51 Pa at 25 ^{0}C ,Water solubility :95 mg/l at 25 ^{0}C .

II. Experimental details

. The fine sample of 14DC2NB was obtained from Sigma Aldrich, UK, and used as such for the spectral measurements. The room temperature FTIR spectrum of the compound was measured in the 4000–400 cm^{-1} region at a resolution of ±1 cm^{-1}, using a BRUKER IFS-66V vacuum Fourier transform spectrometer equipped with a Mercury Cadmium Telluride (MCT) detector, a KBr beam splitter and globar source.

The FT-Raman spectrum of 14DC2NB was recorded on a BRUKER IFS–66V model interferometer equipped with an FRA–106 FT-Raman accessory. The spectrum was recorded in the 3500–50 cm^{-1} Stokes region using the 1064 nm line of a Nd:YAG laser for the excitation operating at 200 mW power. The reported wave numbers are expected to be accurate to within ±1 cm^{-1}.

III. Computational details

The quantum chemical calculation of 14DC2NB has been performed with the standard Density Functional Triply-Parameter Hybrid model DFT/B3LYP. The 6-31G(d,p) basis set have been employed (the valence triple basis set, augmented by d-polarization functions on carbon and nitrogen, p-polarization functions on hydrogen atoms and enlarged by diffuse functions on all atoms) using the Gaussian 09 program [3].The optimized geometry corresponding to the minimum on the potential energy surface have been obtained by solving self consistent field equation iteratively. Harmonic vibrational wavenumbers have been calculated using

analytic second derivatives to confirm the convergence to minima on the potential energy surface and to evaluate the zero-point vibrational energy [4]. Multiple scaling of the force field has been performed by the SQM procedure [5,6] to offset the systematic errors caused by basis set incompleteness, neglect of electron correlation and vibrational anharmonicity [7] These force fields obtained in Cartesian coordinates and dipole derivatives with respect to atomic displacements were extracted from the archive section of the Gaussian 09 output and transformed to a suitably defined set of internal coordinates (the 'natural coordinates'). Normal coordinate analysis on 14DC2NB has been performed to obtain full description of the molecular motion pertaining to the normal modes using the MOLVIB-7.0 program [8,9]

IV. Prediction of Raman intensities

The Raman activities (Si) calculated with the GAUSSIAN 09 program and adjusted during the scaling procedure with MOLVIB were subsequently converted to relative Raman intensities (Ii) using the following relationship derived from the basic theory of Raman scattering [10,11].

$$I_i = \frac{f(\nu_o - \nu_i)^4 S_i}{\nu_i \left[1 - \exp\left(\frac{-hc\nu_i}{kT}\right)\right]}$$

where ν_0 is the exciting frequency (in cm^{-1} units); ν_i is the vibrational wave number of the of the i^{th} normal mode, h, c and k are fundamental constants and f is a suitably chosen common normalization factor for all peaks intensities. Raman activities and calculated Raman intensities are reported in TABLE 5

V. Results and discussion

5.1 Thermodynamic analysis

The molecule taken for this investigation has a great deal of interest in thermodynamic property analysis. Based on the vibrational analysis of title molecule at B3LYP/6-31 G(d,p) basis set ,the thermodynamic parameters such as heat capacity at constant volume(C_V) and Entropy(S) were calculated for different temperatures and listed in the TABLE 1.

It can be seen that, when the temperature increases from 100 to 1000 K the thermodynamic functions like total energies, Specific heat capacity at constant volume (C_V) and Entropy(S) are also increases, because molecular vibrational intensities increase with temperature [12]. The entropy revealed that the molecule possesses more flexibility of changing its own thermodynamic system with respect to the temperature. The correlation graphics of temperature dependence of thermodynamic functions for title molecule are shown in Figures 1.

TABLE 1-The Temperature dependence of Thermodynamic parameters of 14DC2NB

Temperature [T] (K)	Energy [E] (KCal/Mol)	Heat capacity [Cv] (Cal/Mol-Kelvin)	Entropy [S] (Cal/Mol-Kelvin)
100	47.969	16.012	71.715
200	50.117	26.813	87.553
300	51.715	35.692	100.466
400	57.372	44.62	113.359
500	62.159	50.843	124.46
600	65.545	54.123	133.058
700	71.142	57.66	141.985
800	79.299	61.995	152.041
900	85.615	64.238	159.712
1000	92.132	66.05	166.786

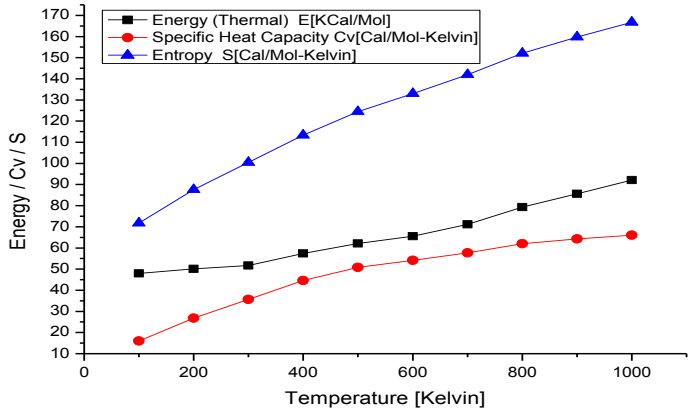

Fig 1. (a). Temperature dependence of Energy [E], Heat Capacity [Cv] and Entropy [S]of 14DC2NB

The zero point vibrational energy and rotational constants in GHz obtained for optimized geometry with B3LYP/6-31 g(d,p) basis set are presented in TABLE2. While performing DFT Calculations the molecule was considered to be at room temperature (298.15K) and at a pressure of 1atm.

TABLE 2-The calculated Thermodynamical parameters of 14DC2NB

Parameters	B3LYP/6-31G(d,p)	
Zero-point vibrational energy (Kcal/Mol)	52.55414	
Rotational constants (GHz):	A	1.37343
	B	0.5541
	C	0.40176

5.2 Molecular geometry

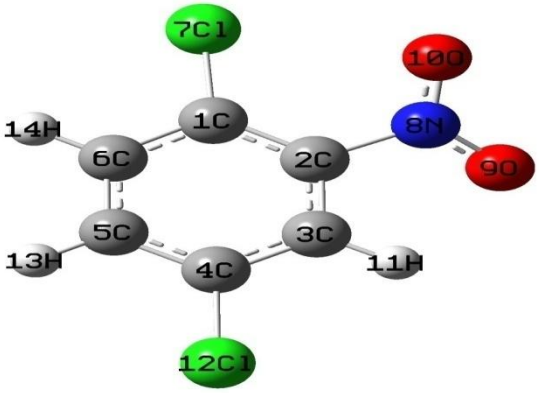

Fig 2. Optimized Structure of 14DC2NB along with numbering of atoms

The labeling of atoms of the title compound is shown in Figure 2. The global minimum energies obtained by the DFT structure optimization for 14DC2NB for B3LYP/6-31G(d,p) , B3LYP/6-311+G(d,p), and B3LYP/6-311G++(d,p) basis sets respectively are presented in TABLE 3. This energy difference is clearly understandable, since the molecules are under different environments.

TABLE 3-Total energies (in Hartrees) based on B3LYP/6-31 g(d,p) , B3LYP/6-311 + G(d,p) and B3LYP/6-311 + +G(d,p) basis sets for 14DC2NB

Basis set	1,4-dichloro-2-nitrobenzene
B3LYP/6-31 G(d,p)	-1355.92910280
B3LYP/6-311+ G(d,p)	-1351.94162484
B3LYP/6-311++ G(d,p)	-1351.94176112

The optimized geometrical parameters like bond length, bond angles and dihedral angles are presented in TABLE 4.

TABLE 4-Optimized geometrical parameters of 14DC2NB obtained by B3LYP/6-31 g(d,p) density functional calculations

Bond length	Angstrum (Å)	Bond angle	Degree	Torsional angle	Degree
C3-H11	1.082178	C1-C6- C 5	121.15	H11-C3-C4-C5	-181.13
C5-H13	1.083941	H11-C3-4C	121.65	H13-C5-C6-C1	-179.35
C6-H14	1.083901	H13-C5-C6	120.3	H14-C6-C1-C2	-180.9
O10-N8	1.22541	H14-C6-C1	118.76	O10-N8-C2-C3	-213.08
O 9- N8	1.23048	O10-N8-C2	118.02	C6-C5-C4-C3	-0.13 4
C4- C3	1.388674	O9-N8-O10	125.38	C1-C6-C5-C4	1.1
C6- C5	1.390993	C4-C3-C2	119.42	C5-C4-C3-C2	-1.14
C1- C6	1.398258	C6-C5-C4	119.47	O9-C2-O10-N8	1.47
C3- C 2	1.395619	C5-C4-C3	120.57	Cl12-C3-C5-4C	0.17
C5- C4	1.395605	N8-C2-C1	123.23	Cl7-C2-C6-C1	2.41
N8- C2	1.476374	Cl7-C1-C6	117.68	N8-C3-C1-C2	0.33
Cl 7- C1	1.740398	Cl12-C4-C5	119.87		
Cl12- C 4	1.749398				

For numbering of atoms refer Fig. 1

1,4-dichloro-2-nitrobenzene(14DC2NB) belongs to C_1 point group symmetry with 14 atoms (N= 14) composing the structure. The molecule has 36 (3N-6) fundamental modes of vibration. From the structural point of view of the molecule 14DC2NB, it has 25 in plane (2N-3) and 11 out of plane vibrations (N-3).

Total number of fundamental modes of vibration, 36 (Γ_{vib}) = 25 A′(in-plane) + 11 A″ (out-of-plane)

5.3 Assignment of the spectra

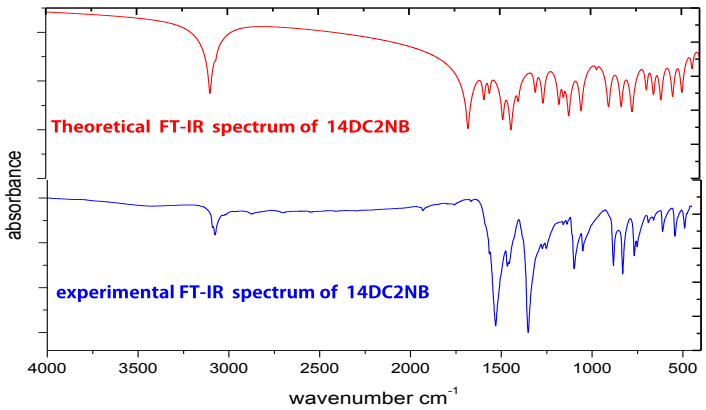

Fig 3. Comparison of Theoretical and experimental FT-IR spectrum of 14DC2NB

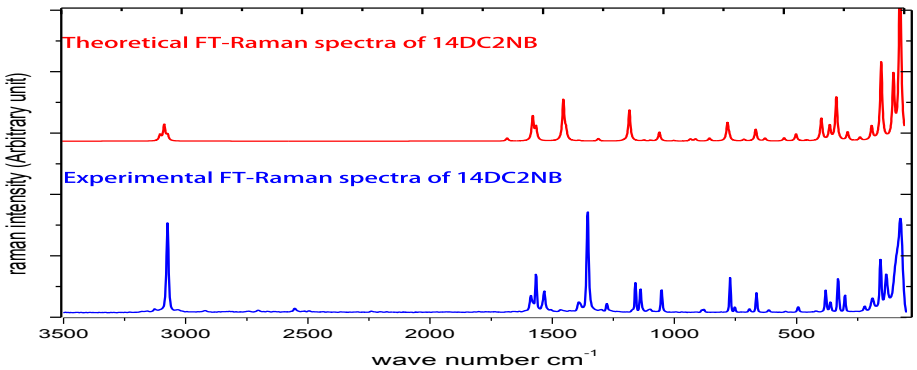

Fig 4. Comparison of Experimental and Theoretical FT-Raman spectrum of 14DC2NB

Detailed description of vibrational modes can be given by means of normal coordinate analysis. The observed and calculated frequencies, calculated IR, Raman and normal mode descriptions (characterized by PED) are reported in Table 5 for 14DC2NB. The observed and simulated FT-IR and FT-Raman spectra of 14DC2NB are presented in Figure 3 and Figure 4 respectively. When using computational methods to predict theoretical normal vibrations for relatively complex polyatomic structures, scaling strategies are used to bring computed wave numbers into closer agreement with observed experimental frequencies using the latest version of MOLVIB program [13].

TABLE 5- Assignment of fundamental vibrations of 14DC2NB by normal mode analysis based on SQM force field calculations using selective scaled B3LYP/6-31g(d,p)

No	Symmetry species	Observed frequency		Calculated using B3LYP/6-31 G(d,p) force field Freq					Characterisation of normal modes with PED%
		IR (cm^{-1})	Raman (cm^{-1})	Unscaled (cm^{-1})	Scaled (cm^{-1})	IR intensity (K mol^{-1})	Raman activity (Si)	Raman intensity (Ii)	
1	A'	3089	-	3251.2	3095.8	7.6517	53.8647	91.0	υCH(99)
2	A'	3076	-	3232.1	3078.5	0.0489	139.7011	240.7	υCH(99)
3	A'	-	3074.4	3219.6	3065	0.1202	49.4697	86.3	υCH(99)
4	A'	1667	-	1663.1	1666.4	157.5665	6.6	76.2	υNO(78), bCNO(14)
5	A'	-	1587.2	1629.6	1600.1	60.315	43.479	528.7	υCC(67), bCH(17),
6	A'	-	1566.1	1606.7	1585.2	18.1316	20.5426	259.0	υCC(74),
7	A'	1456	-	1499.6	1479.9	87.6275	0.6691	10.0	bCH(49), υCC(39),
8	A'	-	1436.9	1423.7	1414.9	2.8521	0.4836	8.3	vCC(53), bCH(28),
9	A'	-	1391	1397.8	1391.3	229.6072	78.1561	1395.0	υNO(73), υCN(14),
10	A'	-	1355	1333.0	1352.4	8.2266	3.9315	78.8	υCC(92)
11	A'	1274	-	1276.6	1262.5	12.2667	0.439	9.8	bCH(71), υCC(17),
12	A'	-	1159.5	1179.5	1161.3	18.3604	15.9016	427.9	bCH(48), vCC(29),
13	A'	1158	-	1152.4	1154.8	9.6758	31.304	890.2	CC(52), CCl(27), bCH(12),
14	A'	1138	-	1121.4	1123.6	48.9362	4.9955	151.5	bCH(39), υCC(29), υCCl(22),
15	A'	-	1052.6	1065.1	1043.3	62.1389	9.3827	321.2	bRing(56),υ CCl(15), υCN(13),
16	A"	951	-	973.0	1054.4	0.336	0.5174	21.9	gCH(88),
17	A"	882	-	910.3	890.2	10.6122	1.9044	93.7	gCH(73), tRing(16)
18	A'	-	879.1	896.5	883	20.2827	1.5174	77.3	bRing(24),υCN(21),υCCl(20),
19	A'	831	-	837.6	818.7	26.3342	2.1892	130.2	gCH(87),
20	A"	-	771.9	779.9	775.3	32.4285	8.2214	574.2	tNO2(59), gCN(14),
21	A'	767	-	770.8	771.4	9.996	1.1964	85.8	bCNO(33), bRing(25),υCCl(22), υCC(13)
22	A"	-	692.8	698.1	691.8	9.0448	1.7834	159.4	tRing(50), gCl(15),
23	A"	-	664	673.6	660.5	1.7392	3.7942	367.1	tRing(32), bRing(30), gCl(10),
24	A'	-	613.8	619.6	618.2	18.8599	1.1343	131.9	vCCl(25),bRing(21),bCNO(18),tRing(15)
25	A"	-	535	544.4	545.1	21.9429	0.5673	87.4	tRing(22),gCl(19),bCNO(17),t NO2(11),
26	A"	-	493.3	501.7	499.1	7.9624	1.8078	332.2	gCl(34),tRing(29),bCCl(10),b CNO(10),
27	A"	490	-	435.6	442.2	0.3085	0.2666	66.3	tRing(54),gCN(13),bCCl(10),
28	A'	-	380.6	383.2	383.8	0.934	3.8409	1253.7	bCNO(24),bRing(21),bCCl(19),CN(13),
29	A"	-	361.5	363.9	357.4	0.739	3.3422	1216.4	bCNO(49), tRing(16), bCCl(12),
30	A'	-	330.1	330.0	329.6	0.0373	8.0173	3584.8	bRing(60), υCCl(23),
31	A"	-	301.9	299.6	288	0.1863	1.2067	660.7	gCl(59), tRing(13),
32	A'	-	221	220.0	237.1	0.0446	0.2765	287.4	bCCl(72), vCC(11),
33	A'	-	189.3	179.2	184.5	1.5756	1.0686	1693.9	bCN(56), bCCl(21), bCNO(11),
34	A"	-	156.5	149.4	149.5	1.2507	3.2698	7527.4	tNO2(64), gCN(19),
35	A"	-	90.9	92.9	120.1	0.5668	1.4654	8865.7	tRing(66), gCl(12),
36	A"	-	74.9	51.3	71.8	0.2337	2.1073	42363.	tNO2(97)

(υ) stretching; (b) bending; (g) scissoring and wagging ; (t) torsion ;PED values greater than 10% are given

The RMS error between unscaled (B3LYP/6-31 G(d,p)) and experimental frequencies are found to be 48.3 cm^{-1}.Root mean square value is obtained in the study using the following expression

$$RMS = \sqrt{\frac{1}{n-1}\sum_{i}^{n}(\upsilon_i^{calcu} - \upsilon_i^{exp})^2}$$

This is quite obvious since the frequencies calculated on the basis of quantum mechanical force fields usually differ appreciably from observed frequencies. This is mainly due to the neglect of anharmonicity and partly due to the approximate nature of the quantum mechanical methods. In order to reproduce the observed frequencies, refinement of scaling factors are applied and optimized via least square refinement algorithm which resulted in a weighted RMS deviation of 9.95 cm^{-1} between the experimental and scaled frequencies .[14]

For 14DC2NB, a multiple scale factors are applied in the normal coordinate analysis and the subsequent least square fit refinement, results into the very close agreement between the observed fundamentals and the scaled frequencies (Table 5). Refinement of the scaling factor applied in this study achieved a weighted mean deviation of 6.49 cm^{-1} between the experimental and SQM frequencies [15-17]. It is convenient to discuss the vibrational spectra of 14DC2NB in terms of characteristic spectral regions as described below.

5.3.1 C-H vibration

Most organic molecules contain alkane residues and their general appearance may be seen in the infrared spectrum. The strong absorption band generally centered around 2925 cm^{-1} represents the C-H stretching absorption of methylene [18] group. Most of the time, it is sufficient to locate the mean position of this aliphatic C-H stretch. In fact, the C-H stretching modes of methylene have asymmetric and symmetric C-H stretching modes and these give four absorption bands just below 3100 cm^{-1}. In our title compound, calculated bands appeared at 3251.2, 3232.1 and 3219.6 cm^{-1} in DFT method have been assigned to C-H asymmetric and symmetric stretching vibrations. The FT-IR bands at 3089 and 3076 cm^{-1} represent C-H stretching vibrations and FT Raman band at 3074.4 cm^{-1} also represents the C-H stretching vibration. The calculated wavenumber for these modes are scaled to 3095.8,3078.5 and 3065 cm^{-1} respectively. The in-plane and out-of-plane bending vibrations of methyl group have also been identified for the title compound and they are presented in Table 5.

5.3.2. C-N vibrations

The C-N stretching frequency is a rather difficult task since the mixing of several bands is possible in this region. In our present work, the band observed at 1390 cm^{-1} in FTIR spectrum and 1052.6 cm^{-1} in Raman spectrum have been attributed to C-N vibrations. The theoretically computed value of the corresponding C-N stretching vibrations is predicted at 1397.8 and 1065 cm^{-1} respectively. These vibrations are mixed with N-O stretching ,Ring bending and C-Cl stretching vibrations as evident from the last column of PED. In this work, the peaks identified at 1356 and 1302 cm^{-1} in IR have been assigned to C-N stretching absorption bands.

5.3.3. C-C vibrations

The C–C aromatic stretching vibrations gives rise to characteristic bands in both the observed IR and Raman spectra, covering the spectral range from 1600 to 1330 cm^{-1}. Generally the C–C stretching vibrations in aromatic compounds are seen in the region of 1400–1650 cm^{-1}. According to Socrates [19], the presence of conjugate substituent such as C–C causes a heavy doublet formation around the region 1625–1575 cm^{-1}. The six ring carbon atoms undergo coupled vibrations which are known as skeletal vibrations give a maximum of four bands in the region 1660–1420 cm^{-1}. In the case of 14DC2NB, the bands observed in IR at 1456 cm^{-1} and those observed in Raman at 1587.2 ,1566.1 1436.9 and 1330.1 have been assigned to C–C stretching vibrations. The calculated C–C stretching vibrations using B3LYP/6-31G(d,p) method are 1499.6, 1587.2, 1566.1 , 1436.9 and 1333 cm^{-1} respectively. The corresponding ring in-plane bending vibrations are shown in Table 5.

5.3.4. C-Cl vibrations

The C–Cl stretching vibrations generally give strong bonds in the region 760-505 cm^{-1} [20]. Vibrational coupling with other groups may result in a shift in the absorption as high as 840 cm^{-1} [21]. Based on the Raman band at 613.8 cm^{-1} has been assigned to C–Cl stretching, this was also confirmed by TED output. Most of the aromatic chloro compounds have a band of strong-to-medium intensity in the region 385–265 cm^{-1} due to C-Cl in-plane bending vibrations . Accordingly the Raman band identified at 380.6 cm^{-1} has been assigned to the C-Cl in-plane bending mode. The C-Cl out of plane deformation vibrations have been established at 302 and 91 cm^{-1} in Raman spectrum.

5.4 Frontier molecular orbitals

Both the Highest Occupied Molecular Orbital (HOMO) and the Lowest Unoccupied Molecular Orbital (LUMO) are the main orbital taking part in chemical reaction. Determination of energies of the HOMO and LUMO are important parameters in quantum chemical calculations [22–25]. The HOMO energy characterizes the ability of electron giving, the LUMO characterizes the ability of electron accepting, and the gap between HOMO and LUMO characterizes the molecular chemical stability [26]. The energy gap between the HOMOs and LUMOs called as energy gap .It is a critical parameter in determining molecular electrical transport properties since it is a measure of electron conductivity [27]. In order to evaluate the energies behavior of the title compounds energies of HOMO, LUMO and their orbital energy gaps were calculated by B3LYP/6-31g(d,p) method and it is given in Table 7. The 3D plots of the frontier orbitals in the ground state HOMO and the exited state LUMO, are shown in Figure. 5 . The energy gap HOMO–LUMO explains the eventual charge transfer interaction within the molecule, which influences the biological activity of the molecule.

This electronic absorption corresponds to the transition from the ground state to the first excited state and is mainly described by one electron excitation from HOMO to LUMO. While the energy of the HOMO is directly related to the ionization potential, LUMO energy is directly related to the electron affinity.

There are lots of applications available for the use of HOMO and LUMO energy gap as a quantum chemical descriptor. It establishes correlation in various chemical and bio-chemical systems [28]. The HOMO–LUMO energy gap is an important value for stability index. A large HOMO–LUMO gap implies high stability for the molecule in the sense of its lower reactivity in chemical reactions [29]. According to B3LYP/6-31G(d,p) calculation, the energy band gap (translation from HOMO to LUMO) of the molecule is about - 4.270317eV

HOMO energy	=	**- 7.227401eV**
LUMO energy	=	**- 2.957084 eV**
HOMO – LUMO energy gap	=	**- 4.270317Ev**

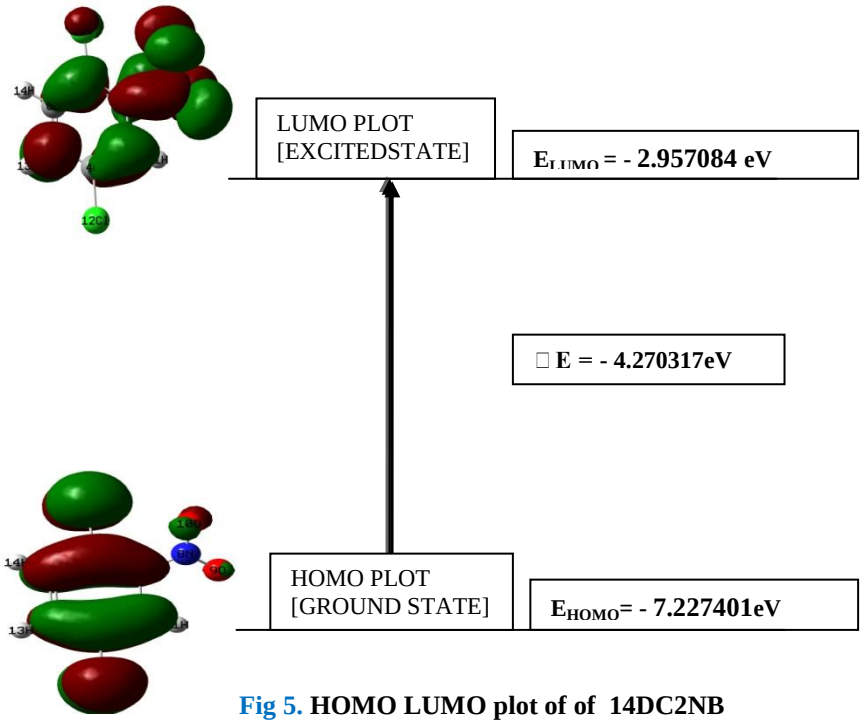

Fig 5. HOMO LUMO plot of of 14DC2NB

5.5. Global reactivity descriptors

By using HOMO and LUMO energy values for a molecule, the global chemical reactivity descriptors of molecules such as hardness (η), chemical potential (μ), softness (S), electronegativity (χ) and electrophilicity index (ω) have been defined [29,30].On the basis of E_{HOMO} and E_{LUMO}, these are calculated using the below equations.

Using Koopman's theorem for closed-shell molecules,

The hardness of the molecule is[31]

$$\square = (I - A) / 2$$

The chemical potential of the molecule is

$$\square = -(I + A)/2$$

The softness of the molecule is **S = 1/2** □
The electronegativity of the molecule is

□ =$(I + A)$ / 2

The electrophilicity index of the molecule is

□ = □²/2 □

Where I is the ionization potentional and A is the electron affinity of the molecule. I and A can be expressed through HOMO and LUMO orbital energies as I = - E_{HOMO} and A = - E_{LUMO}. The ionization potentional I and an electron affinity A of our molecule 14DC2NB calculated by B3LYP/ 6-31G(d,p) method is 7.2274 eV and 2.9571 eV respectively.

TABLE 6.Energy values of 14DC2NB by B3LYP/6 31g(d,p) method

Energies	values
E_{HOMO} (eV)	-7.2274
E_{LUMO} (eV)	-2.9571
E_{HOMO} - E_{LUMO} gap (eV)	-4.2703
Ionization Potentional (I)	7.2274
electron affinity (A)	2.9571
Chemical hardness (η)	2.1352
Softness (S)	0.2342
Chemical potential (μ)	-5.0922
Electronegativity (χ)	1.6923
Electrophilicity index (ω)	5.0922

The calculated values of the Chemical Hardness, Softness, Chemical potential, Electronegativity and Electrophilicity index of our molecule 14DC2NB is 2.1352, 0.2342, -5.0922, 1.6923 and 5.0922 respectively as shown TABLE 6 . Considering the chemical hardness, large HOMO-LUMO gap represent a hard molecule and small HOMO-LUMO gap represent a soft molecule. From the Table 9, it is clear that the molecule under investigation is very hard since it has a large HOMO-LUMO gap and also having a very small value for softness.

5.6. ^{13}C and ^{1}H NMR spectral analysis

Recently, Gauge Invariant Atomic Orbital's (GIAO) NMR DFT calculations have become popular [32] and can successfully predict the chemical shift (d, ppm) for small isolated molecules [33-35]. However, the accuracy of NMR theoretical predictions depend on the implemented basis set, and optimized structural parameters. Earlier investigations favor DFT predictions over the RHF method [36]. Therefore, structural parameters obtained with the hybrid B3LYP functional at the 6-31G(d,p) level of theory were used to predict ^{1}H and ^{13}C chemical shifts utilizing the recommended GIAO approach [37]. The theoretically computed ^{13}C and ^{1}H NMR spectrum are shown in Figure 6. Chemical shifts were reported in parts per million relative to TMS. Relative chemical shifts were estimated by using the corresponding TMS shielding calculated in advance at the same theoretical level as the reference. Aromatic carbons give signals in overlapped areas of the spectrum with chemical shift values from 100 to 150 ppm [38,39]. It can be seen from Table 6, that due to the influence of electronegative nitrogen atom, the chemical shift value of carbon atoms are significantly differing the shift positions in the range 120–150 ppm. Thus, the C2 atom has its chemical shifts at 149.9479 ppm. The chemical shift values of H atoms in methyl group are quite low (≤8ppm) due to the shielding effect. The chemical shift values of Carbon and Hydrogen atoms are reported in TABLE 7.

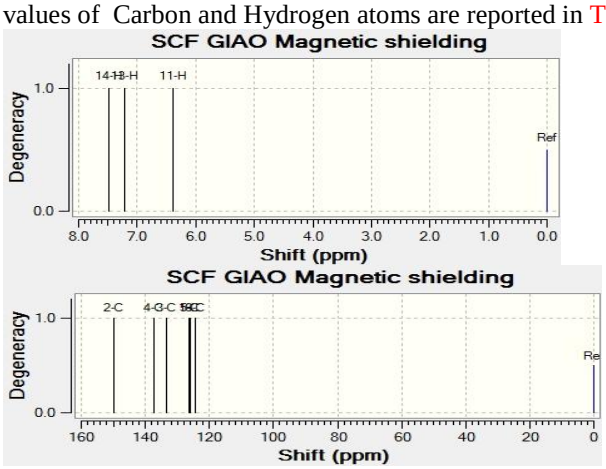

Fig 6. Theoretically calculated NMR Spectrum of ^{1}H and ^{13}C of 14DC2NB

TABLE 7. Theoretical isotropic chemical shift calculated using DFT B3LYP/6-31 G(d,p) (with respect to TMS, All values in ppm) for 14DC2NB

Calculated chemical shift (ppm)	
Atom	**B3LYP/6-31G(d,p)**
C1	126.3355
C2	149.9479
C3	133.5804
C4	137.1584
C5	125.868
C6	124.2161
H11	7.4826
H13	7.219
H14	6.3927

For numbering of atoms refer Fig. 1

5.7 Natural atomic charge analysis:Mullikan's population analysis

Natural bond orbital analysis provides an efficient method for studying intra and intermolecular bonding and interaction among bonds, and also provides a convenient basis for investigating charge transfer in molecular system. Atomic charges of 14DC2NB molecule have been calculated by DFT method shown in Table 8. The magnitude of the carbon atomic charges is found to be positive and negative. The magnitude of the hydrogen atomic charges is found to be only positive and arranged in an order from 0.1321 to 0.1614 for 14DC2NB, indicating the charge transfer from H to carbon atom. Additionally the magnitudes of atomic charge of both O atoms are positive and atomic charge of N was noted to be only negative value, indicating the charge transfer from Nitrogen atom to Oxygen atom. Mullikan's population analysis provides [40] partitioning of either a total charge density or an orbital density. Mullikan's atomic charges of 14DC2NB molecule have been calculated by DFT method is shown in Figure 7 and the histogram of calculated mulliken charges of 14DC2NB is shown in Figure .8

.

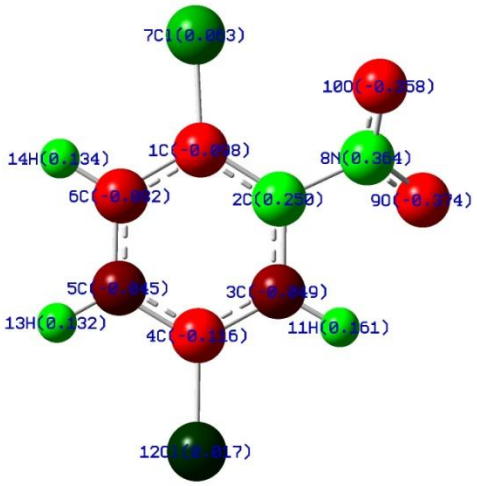

Fig 7.Illustration of mullikken atomic charges

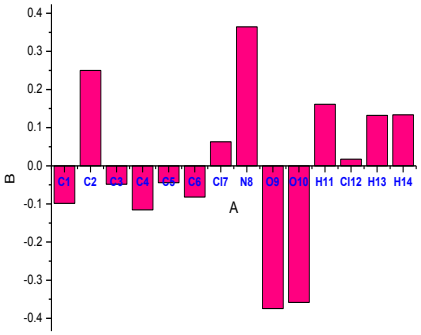

Fig 8.Histogram of mullikan charges of 14DC2NB

TABLE 8. Atomic charges for optimized geometry of 14DC2NB using DFT B3LYP/6-31g(d,p)

Atomic Number	1,4-dichloro-2-nitrobenzene
	Mulliken atomic charges
C1	-0.0983
C2	0.2498
C3	-0.0485
C4	-0.1157
C5	-0.0446
C6	-0.0819
Cl7	0.0628

N8	0.3644
O9	-0.3744
O10	-0.3583
H11	0.1614
Cl12	0.0173
H13	0.1321
H14	0.1339

For numbering of atoms refer Fig. 1

5.8 UV-Vis spectral analysis

The Time Dependant Density Functional Theory(TD-DFT) Calculation has been performed for 14DC2NB on the basis of fully optimized ground state structure to investigate the electronic absorption properties[41-44]. TD-DFT is able to detect accurate absorption wavelengths at a relatively small computing time which correspond to vertical electronic transitions computed on the ground state geometry, especially in the study of solvent effect [45–47]; Thus TD-DFT method is used with B3LYP function and 6-31G(d,p) basis set for vertical excitation energy of electronic spectra. The calculated visible absorption maxima of wave length λ which are a function of the electron availability have been reported in Table 9.

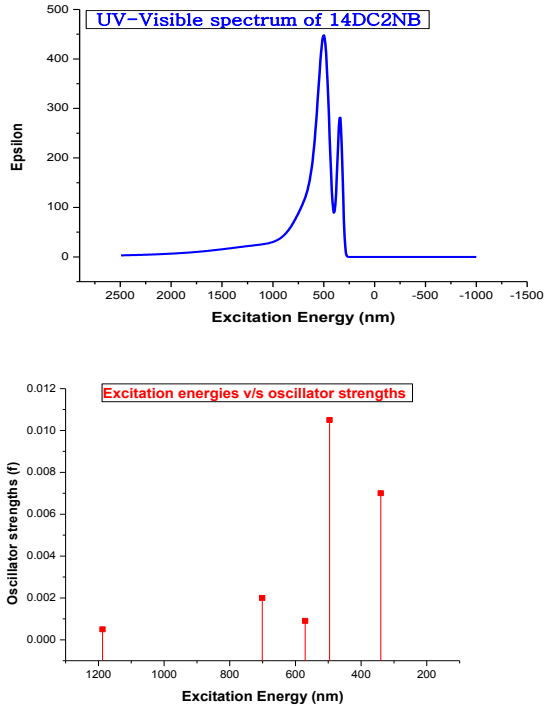

Fig.9. The UV-Visible spectrum and excitation energy v/s oscillator strength of 14DC2NB

The excitation energies, wave length and oscillator strengths for the title molecule at the optimized geometry in the ground state were obtained in the frame work of TD-DFT calculations with the B3LYP/6-31G(d,p) method. TD-DFT methods are computationally more expensive than semi-empirical methods but allow easily studies of medium size molecules [48-50]. The computed UV spectra predicts one intense electronic transition at 496.16 nm with an oscillator strength f = 0.0105 a.u and another electronic transition at 340.21 nm with an oscillator strength f = 0.007 a.u .Calculations of molecular orbital geometry show that the visible absorption maxima of title molecule correspond to the electron transition between frontier orbitals such as transition from HOMO to LUMO. The λ_{max} is a function of substitution. The stronger the donor character of the substitution, the more electrons pushed into the molecule, the larger λ_{max}. These values may be slightly shifted by solvent effects. The role of substituent and role of the solvent influence the UV-Visible spectrum. This band may be due to electronic transition of the ring to methyl group (transition of π-π*). Both the (HOMO) and (LUMO) are the main orbitals that take part in chemical stability [51].

The theoretical electronic excitation energies ,wavelength of the excitation and oscillator strengths were calculated and listed in TABLE 9 and the Theoretical UV-Visible spectrum and excitation energy v/s oscillator strength of 14DC2NB is shown in Figure.9

TABLE 9.Theoretical electronic absorption spectra values of 14DC2NB

Excited State	Energy (eV)	Wavelength □ (nm)	Oscillator strengths (f)
Excited State:1	1.0441	1187.52	0.0005
Excited State:2	1.7691	700.83	0.002
Excited State:3	2.1732	570.52	0.0009
Excited State:4	2.4989	496.16	0.0105
Excited State:5	3.6443	340.21	0.007

5.9 Analysis of molecular electrostatic surface potential

The electrostatic potential generated in space by charge distribution is helpful to understand the electrophilic and nucleophilic regions in the title molecule. The molecular electrostatic surface potential provides a visual method to understand the relative polarity of compounds[51-52]. Electrostatic potential map illustrates the charge distributions of the molecule three dimensionally. One of the purposes of finding the electrostatic potential is to find the reactive site of a molecule [53,54]. Knowledge of the charge distributions can be used to determine how molecules interact with one another. In the electrostatic potential map, the semispherical blue shapes that emerge from the edges of the above electrostatic potential map are hydrogen atoms. The molecular electrostatic potential (MEP) at a point r in the space around a molecule (in atomic units) can be expressed as

$$V(r) = \sum_A \frac{Z_A}{|\vec{R}_A - \vec{r}|} - \int \frac{\rho(\vec{r}')}{|\vec{r}' - \vec{r}|} d\vec{r}'$$

Where Z_A is the charge of nucleus A located at R_A, $\rho(\vec{r}')$ is the electronic density function of the molecule, and $\vec{r}'$ is the dummy integration variable

The first and second term represent the contributions to the potential due to nuclei and electron respectively. V(r) is the net resultant electrostatic effect produced at the point r by both the electrons and nuclei of the molecule.

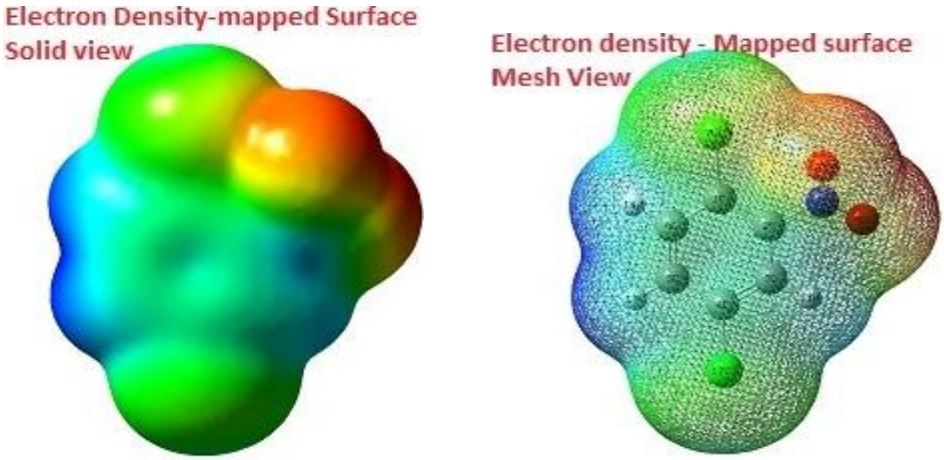

Fig 10. Total electron density isosurface mapped with molecular electrostatic potential of 14DC2NB (solid view and mesh view)

These two figures, Figure.10 (a) mesh view and (b) solid view illustrate an electron density mapped surface of our title compound.Molecular electrostatic surface potential (MESP) at a point in a space around a molecule gives an indication of the net electrostatic effect produced at that point by total charge distribution (electron +nuclei) of the molecule and correlates with dipole moments, electro negativity, partial charges and chemical reactivity of the molecule. Potential increases in the following order with respect to the colour. Red < yellow < green < blue. That is negative region (blue and yellow) are related to electrophilic reactivity .The maximum positive regions are localized on the oxygen atom of nitro group which can be considered as possible sites for nucleophilic attack. That is negative potential sites are on the electronegative atoms while the positive potential sites around oxygen atoms. Green area covers parts of the molecule where electrostatic potentials are nearly equal to zero (C-Cl bond). This is a region of zero potential enveloping the π systems of aromatic ring leaving a more electrophilic region in the plane of hydrogen atom.[54]. The contour map of positive and negative potential is shown in Figure 11.

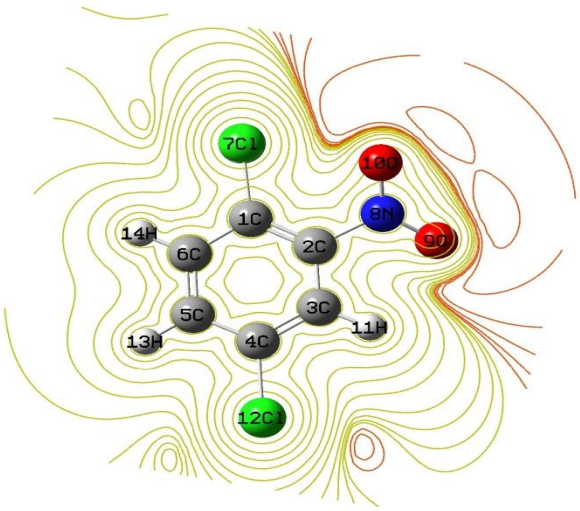

Fig 11. Contour map of molecular electrostatic potential surface of 14DC2NB

VI. Conclusion

The vibrational properties and electronic properties of 14DC2NB have been investigated by FT-IR and FT-Raman spectroscopy and were performed accordingly to the SQM force field method based on the ab-initioB3LYP/6-31g(d,p) level. The molecular geometry, vibrational frequencies, infrared intensities, Raman intensities and Raman activities of 14DC2NB are calculated. The theoretically calculated vibrational modes are compared with experimental values. The experimental values are in good agreement with theoretical values even in the low frequency region. The differences between the observed and scaled wavenumber values of most of the fundamentals are very small. The thermodynamic properties (The Energy, heat capacity at constant volume and entropy) in the temperature ranges from 100 to 1000 K ,Rotational constants, a zero point vibrational energy and SCF energy of title compound are also calculated. The theoretical UV-Visible spectrum was recorded. The ^{1}H and ^{13}C NMR magnetic isotropic chemical shifts were calculated by B3LYP/6-31 g(d,p) basis set . Natural bond orbital analysis – Mullikkan population analysis also carried out. The difference in HOMO and LUMO energy supports the interaction of charge transfer within the molecule. The MEP map shows that the negative potential sites are around hydrogen atoms as well as the positive potential sites are around the oxygen atoms.

Acknowledgement

The authors are thankful to Sophisticated Analytical Instrumentation Facility (SAIF), IIT, Chennai, for the spectral measurements.

REFERENCE

[1] J Senthil kumar et al Ind.Jour. of Pure n appli. Phy. Vol.49 oct 2011 pp 673-678
[2] Krishna Kumar V & Prabhavathi N, Spectrochem. Acta A 72(2009) 738.
[3] M.J. Frisch, G.W. Trucks, H.B. Schlegel, G.E. Scuseria, M.A. Robb, J.R. Cheeseman, G. Scalmani, V. Barone, B. Mennucci, G.A. Petersson, H. Nakatsuji, M.Caricato, X. Li, H.P. Hratchian, A.F. Izmaylov, J. Bloino, G. Zheng, J.L. Sonnenberg, M. Hada, M. Ehara, K. Toyota, R. Fukuda, J. Hasegawa, M. Ishida, T. Nakajima, Y. Honda, O. Kitao, H. Nakai, T. Vreven, J.A. Montgomery Jr., J.E. Peralta,F.Ogliaro,M. Bearpark, J.J. Heyd, E. Brothers, K.N. Kudin, V.N. Staroverov, R. Kobayashi, J.Normand, K. Raghavachari, A. Rendell, J.C. Burant, S.S. Iyengar, J. Tomasi, M.Cossi, N. Rega, J.M. Millam, M. Klene, J.E. Knox, J.B. Cross, V. Bakken, C. Adamo, J. Jaramillo, R. Gomperts, R.E. Stratmann, O. Yazyev, A.J. Austin, R. Cammi, C. Pomelli,J.W. Ochterski, R.L. Martin, K. Morokuma, V.G. Zakrzewski, G.A. Voth, P. Salvador,J.J. Dannenberg, S. Dapprich, A.D. Daniels, O. Farkas, J.B. Foresman, J.V. Ortiz, J. Cioslowski, D.J. Fox, Gaussian Inc., Wallingford, CT, 2009.
[4] V. Mukherjee, N.P. Singh, R.A. Yadav, J. Mol. Struct. 988 (2011) 24–34.
[5] G. Rauhut, P. Pulay, J. Phys. Chem. 99 (1995) 3093–3100.
[6] P. Pulay, G. Fogarasi, G. Pongor, J.E. Boggs, A. Vargha, J. Am. Chem. Soc. 105 (1983) 7037–7047.
[7] G. Fogarasi,P. Pulay, in:J.R.Durig (Ed.),Vibrational Spectra and Structure, vol.14, Elsevier, Amsterdam, 1985, pp. 125–219.
[8] T. Sundius, J. Mol. Struct. 218 (1990) 321–326.
[9] T. Sundius, Vib. Spectrosc. 29 (2002) 89–95..
[10] P.S.Kalsi, Spectroscopy of Organic Compounds, Sixth ed., New Age International (p) Limited Publishers, New Delhi, 2005.
[11] G. Socrates, Infrared and Raman Characteristic group frequencies, Tables and Charts,third ed., Wiley, Chichester, 2001.
[12] J.B. Ott, J. Boerio-Goates, Chemical Thermodynamics: Advanced Applications, Calculations from Statistical Thermodynamics, Academic Press 2000.
[13] N.Prabhavathi,A.Nilufer ,V.Krishnakumar Spectrochem. Acta Part A Mol. Biomol. Spectrosc. .114(2013) 101-113
[14] S.Seshadri, Rasheed.M.P ,R.Sangeetha ,Int.J.Scie.Res. Appl.Chem 8(2015) 87-100
[15] P.S.Kalsi, Spectroscopy of Organic Compounds, Sixth ed., New Age International (p) Limited Publishers, New Delhi, 2005
[16] G. Socrates, Infrared and Raman Characteristic group frequencies, Tables and Charts, third ed., Wiley, Chichester, 2001

[17] F.R. Dollish, W.G. Fateley, F.F. Bentley, Characteristic Raman Frequencies of Organic Compounds, John Wiley & Sons, New York, 1997.
[18] G. Fogarasi, X. Zhou, P.W. Taylor,P. Pulay,J. Am. Chem. Soc. 114(1992) 8191– 8201.
[19] D.N. Sathyanarayana, Vibrational Spectroscopy Theory and Application, New Age International Publishers, New Delhi, 2004
[20] S. George, Infrared and Raman Characteristic Group Frequencies Tables and Charts, 3rd ed., Wiley, Chichester, 2001.
[21] B. Lakshmaiah, G. Ramana Rao, J. Raman Spectrosc. 20 (1989) 439.
[22] I. Fleming, Frontier Orbitals and Organic Chemical Reactions, John Wiley & Sons, New York, 1976. pp. 5–27.
[23] J.S. Murray, K. Sen, Molecular Electrostatic Potentials, Concepts and 399 Applications, Elsevier, Amsterdam, 1996.
[24] Fleming, Ian, Frontier Orbital Organic Chemical Reactions, Wiley, London,1978.
[25] R. Ditchfield, J. Chem. Phys. 56 (1972) 5688–5703.
[26] D.Lin-vien, N.B. Cothup, W.G. Fateley, J.G. Graselli, The Handbook of Infrared and Raman Characteristic Frequencies of Organic Molecules, Akademic Press,Boston, 1991.
[27] C. James, C. Ravikumar, T. Sundius, V. Krishnakumar, R. Kesavamoorthy, Jayakumar, I. Hubert Joe, Vib. Spectrosc. 47 (2008) 10–20
[28] J.M.Seminario, Recent Developments and Applications of Modern Density Functional Theory, vol. 4, Elsevier, Amsterdam, 1996
[29] S. Gunasekaran, R.A. Balaji, S. Kumeresan, G. Anand, S. Srinivasan, Can. J. Anal. Sci. Spectrosc. 53 (2008) 149-161.
[30] D.A. Kleinman, Phys. Rev. 126 (1962) 1977–1979.
[31] K. Fukui, Science 218 (1982) 747–754.
[32] Mehmet Karabacak, Mehmet Cinar, Mustafa Kurt, Spectrochim. Acta Part A Mol. Biomol. Spectrosc. 74 (2009) 1197–1203.
[33] D.F.V. Lewis, C. Loannides, D.V. Parke, Xenobiotica 24 (1994) 401–408.
[34] Z. Zhou, R.G. Parr, J. Am. Chem. Soc. 112 (1990) 5720–5724
[35] A.D. Becke, Phys. Rev. 38A (1988) 3098–3100.
[36] V.G. Malkin, O.L. Malkina, M.E. Casida, D.R. Salahub, J. Am. Chem. Soc. 116 (1994) 5898–5908.
[37] Z. Parr, L. Szentpaly, S. Liu, Am. Chem. Soc. 121 (1999) 1922–1924
[38] T. Kupka, M. Kolaski, G. Pasterna, K. Ruud, J. Mol. Struct. THEOCHEM 467 (1999) 63–78.
[39] T. Kupka, G. Pasterna, P. Lodowski, W. Szeja, Magn. Reson. Chem. 37 (1999) 421–426.
[40] H.O. Kalinowski, S. Berger, S. Braun, Carbon-13 NMR Spectroscopy, John Wiley&Sons, Chichester, 1988.
[41] K. Pihlaja, E. Kleinpeter (Eds.), Carbon-13 Chemical Shifts in Structural and Sterochemical Analysis, VCH Publishers, Deerfield Beach, 1994.
[42] D. Arul Dhas, I. Hubert Joe, S.D.D. Roy, T.H. Freeda, Spectrochim. Acta 77 (2010) 36–44.
[43] K. Jug, Z.B. Maksic, in: Z.B. Maksic (Ed.), Theoretical Model of Chemical Bonding, Part 3, Springer, Berlin, 1991, pp. 233–236.
[44] S. Fliszar, Charge Distributions and Chemical Effects, Springer, New York, 1983.
[45] J. Gao, J. Chem. Phys. 98 (1993) 1975–1981.
[46] P. Cieplak, J. Comp. Chem. 12 (1991) 1232–1236.
[47] M. Kurt, P. Chinna Babu, N. Sundaraganesan, M. Cinar, M. Karabacak, Spectrochim. Acta Part A Mol. Biomol. Spectrosc. 79 (2011) 1162–1170.
[48] D. Jacquemin, J. Preat, M. Charlot, V. Wathelet, J.M. Andre, E.A. Perpete, J. Chem. Phys. 121 (2004) 1736-1744.
[49] M. Cossi, V. Barone, J. Chem. Phys. 115 (2001) 4708-4717.
[50] D. Guillaumont, S. Nakamura, Dyes Pigments 46 (2000) 85–92.
[51] J. Fabian, Dyes Pigments 84 (2010) 36–53
[52] R.H. Petrucci, W.S. Harwood, F.G. Herring, J.D. Madura, General Chemistry: Principles & Modern Applications, ninth ed., Pearson Education Inc., New Jersey, 2007.
[53] P. Chattraj, B. Maiti, U. Sarkar, J. Phys. Chem. A107 (2003) 4973–4975.
[54] S.Seshadri, Rasheed.M.P ,R.Sangeetha ,IOSR-J. Appl.Chem 8(2015) 87-100